Purdue University
Purdue e-Pubs

12-31-2013

Optical Properties of Gallium-Doped Zinc Oxide-A Low-Loss Plasmonic Material: First-Principles Theory and Experiment

Jongbum Kim
Birck Nanotechnology Center, Purdue University, kim668@purdue.edu

Gururaj V. Naik
Purdue University, Birck Nanotechnology Center, gnaik@purdue.edu

Alexander V. Gavrilenko
Norfolk State University

Krishnaveni Dondapati
Norfolk State University

Vladimir I. Gavrilenko
Norfolk State University

See next page for additional authors

Follow this and additional works at: http://docs.lib.purdue.edu/nanopub
Part of the Nanoscience and Nanotechnology Commons

Authors

Jongbum Kim, Gururaj V. Naik, Alexander V. Gavrilenko, Krishnaveni Dondapati, Vladimir I. Gavrilenko, S. M. Prokes, O. J. Glembocki, V. M. Shalaev, and Alexandra Boltasseva

Optical Properties of Gallium-Doped Zinc Oxide—A Low-Loss Plasmonic Material: First-Principles Theory and Experiment

Jongbum Kim,[1] Gururaj V. Naik,[1] Alexander V. Gavrilenko,[2] Krishnaveni Dondapati,[2] Vladimir I. Gavrilenko,[2] S. M. Prokes,[3] Orest J. Glembocki,[3] Vladimir M. Shalaev,[1] and Alexandra Boltasseva[1]

[1]*Birck Nanotechnology Center and School of Electrical & Computer Engineering, Purdue University, West Lafayette, Indiana 47907, USA*
[2]*Center for Materials Research, Norfolk State University, 700 Park Avenue, Norfolk, Virginia 23504, USA*
[3]*Electronic Science Division, Naval Research Laboratory, Washington, D.C. 20375, USA*

Searching for better materials for plasmonic and metamaterial applications is an inverse design problem where theoretical studies are necessary. Using basic models of impurity doping in semiconductors, transparent conducting oxides (TCOs) are identified as low-loss plasmonic materials in the near-infrared wavelength range. A more sophisticated theoretical study would help not only to improve the properties of TCOs but also to design further lower-loss materials. In this study, optical functions of one such TCO, gallium-doped zinc oxide (GZO), are studied both experimentally and by first-principles density-functional calculations. Pulsed-laser-deposited GZO films are studied by the x-ray diffraction and generalized spectroscopic ellipsometry. Theoretical studies are performed by the total-energy-minimization method for the equilibrium atomic structure of GZO and random phase approximation with the quasiparticle gap correction. Plasma excitation effects are also included for optical functions. This study identifies mechanisms other than doping, such as alloying effects, that significantly influence the optical properties of GZO films. It also indicates that ultraheavy Ga doping of ZnO results in a new alloy material, rather than just degenerately doped ZnO. This work is the first step to achieve a fundamental understanding of the connection between material, structural, and optical properties of highly doped TCOs to tailor those materials for various plasmonic applications.

I. INTRODUCTION

In the past decade, there have been many breakthroughs in the field of plasmonics and metamaterials that have enabled optical devices with unprecedented functionalities [1–4]. Many of these devices have remained in research laboratories without being realized in commercial production lines because of many technological hurdles. One such major problem haunting plasmonic and metamaterial devices is the high optical losses in plasmonic building blocks [5]. Typical plasmonic components such as gold or silver nanostructures exhibit large optical loss in the visible and near-infrared regions. Additionally, gold and silver have other drawbacks, such as difficulty in fabricating nanostructures, incompatibility with well-established processes like silicon complementary metal-oxide-semiconductor, and relatively low thermal and/or chemical stabilities. Hence, there is a need for finding better alternatives to gold and silver [5].

Finding a low-loss metallic component for a given plasmonic or metamaterial application is a complex inverse-design problem. Hence, various simplified approaches have been attempted to produce low-loss metallic components. Given the fact that so far it has not been possible to realize a bulk zero-loss metal [6], reducing losses in plasmonic materials to a tolerable extent is a practical solution that is being pursued by many research groups (for a recent review, see Ref. [7] and references therein). One of the approaches is to tailor the carrier concentration of the plasmonic material to a moderate value [8]. Optical loss characterized by the imaginary part of permittivity is proportional to the carrier concentration of a plasmonic material. Hence, reducing carrier concentration of metals to a moderate value is one of the approaches in achieving low-loss plasmonic material. Using this approach, heavily doped semiconductors such as indium tin oxide (ITO), aluminum-doped zinc oxide (AZO), and gallium-doped zinc oxide (GZO) are shown to be low-loss plasmonic materials in the near infrared [9–11]. Recently, indium-doped cadmium oxide (ICO), another type of TCO, was also demonstrated as a low-loss plasmonic material in the near infrared [12]. TCOs exhibit losses nearly 5 times smaller than that of the best metal (Ag) in the near-infrared range, where they turn out to be plasmonic. Figure 1 plots the optical loss or imaginary permittivity (ε'') of AZO, GZO, and ITO, along with that of noble metals, gold, and
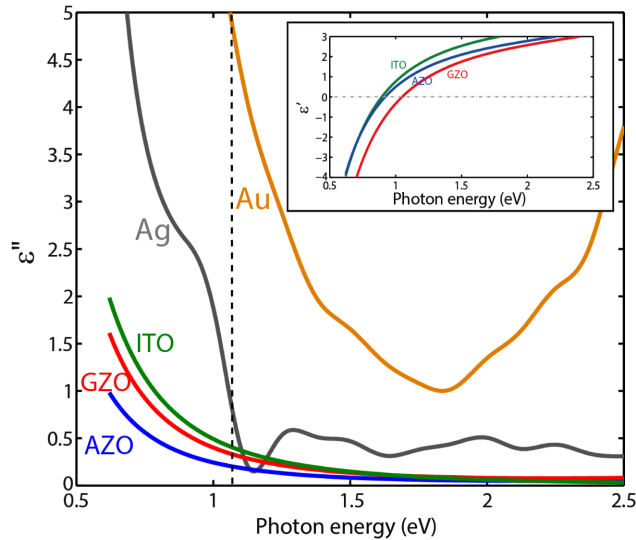
FIG. 1 (color online). Optical loss or imaginary part of permittivity of three transparent conducting oxides: ITO, AZO, and GZO, compared with that of gold and silver. Optical constants of thin films of AZO, GZO, and ITO are from Ref. [13], and those of gold and silver are from Ref. [14]. The inset shows the real part of permittivity of AZO, GZO, and ITO. The vertical dashed line corresponds to the photon energy where real permittivity of GZO crosses zero.
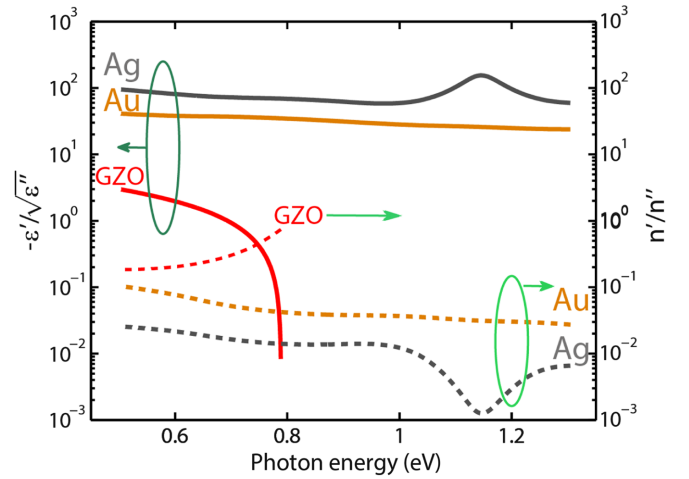

FIG. 2 (color online). FoM of LSPR and surface plasmon polariton waveguiding devices (solid lines) and TO devices (dashed lines) calculated for GZO, gold, and silver as plasmonic materials.

silver. It may be noted that smaller imaginary permittivity or optical loss does not necessarily mean better performance of a plasmonic or metamaterial device.

In general, the device performance depends on both the real and imaginary parts of permittivity. The performance of plasmonic devices can be quantified based on the figure of merit (FoM), which forms a common platform to evaluate the performance of various materials used in different applications over a wide frequency band, as suggested in Ref. [15]. Adopting the general FoM definition for localized surface-plasmon resonance (LSPR) applications as $|\mathrm{Re}(\varepsilon)|/\sqrt{\mathrm{Im}(\varepsilon)}$, the efficiency of various plasmonic materials can be evaluated [15]. The same FoM holds for any of the surface plasmon polariton waveguiding applications as well. Figure 2 plots this quantity for GZO, gold, and silver. Generally speaking, gold and silver outperform TCOs for these applications. Nevertheless, TCOs are good alternatives in the near infrared for simple device geometries [7]. Figure 2 also plots the FoM for transformation optics (TO) devices, which can be defined as the ratio of the real part of the refractive index (n') to the imaginary part (n''). From this plot, we can clearly see that TCOs are promising candidates as plasmonic materials in the near infrared for nonresonant applications such as TO devices. Devices such as epsilon-near-zero and hyperbolic metamaterials do benefit significantly by using TCOs as their plasmonic components.

The optical properties of TCOs may be further improved if their electronic band structure is engineered to achieve

lower optical loss. Engineering the electronic band structure of materials to design plasmonic materials was demonstrated earlier with alkali-noble intermetallics and gold-cadmium alloys [16,17]. This approach requires theoretical studies using techniques such as density functional theory (DFT) in order to predict the optical properties of the "designer" plasmonic material. This approach may be applied to TCOs, and many other good plasmonic materials as well, to improve their optical properties and also gain better insight into solving the complex inverse design problem of finding low-loss plasmonic materials.

More detailed analyses on a comparison study of alternative materials can be found in Sec. 8 of Ref. [7]. Analyses have shown that TCOs are promising candidates as plasmonic materials in the near-infrared and longer wavelengths for devices based on epsilon-near-zero (ENZ), hyperbolic metamaterials, localized surface-plasmon resonance, and tunable devices.

In this work, we apply electronic band-structure calculations to study the optical properties of GZO. Among the three TCOs considered, GZO can be doped to achieve the highest carrier concentration in spite of the smaller solid-solubility limit of Ga in ZnO [18]. The optical properties of heavily doped GZO possess nontrivial dependence on the doping concentration, especially when doped as close to the solid-solubility limit as possible. Though there are many reports that study the electronic or optical properties of heavily doped GZO films [19–22], it is not well understood how the carrier concentration, crystallinity of films, and alloying effects influence the optical properties. Here, we use first-principles DFT to study the influence of each of these factors on the optical properties of plasmonic GZO films. Theoretical studies are supported with experimental studies on high-quality n-type wurtzite ZnO ($w-$ZnO) polycrystalline films doped with gallium.

TABLE I. Typical deposition parameters for 3 wt% and 6 wt% GZO.

Doping density	3 wt%	6 wt%
Ratio of pulses (ZnO : Ga_2O_3)	60: 1	30: 1
Ablation rate (Hz)	1	1
Oxygen partial pressure (Torr)	10^{-3}	10^{-3}

First-principles DFT calculations are incorporated to study the electron energy structure and optical functions of heavy Ga-doped wurtzite ZnO crystals. The ground states of the systems are obtained by the total energy minimization method within the local density approximation (LDA). The effects of Ga doping on the electron energy structure and optical functions are presented.

II. SAMPLE PREPARATION AND CHARACTERIZATION

Pulsed laser deposition (PLD) is a growth technique for thin films by condensation of laser plasma ablated from multiple targets excited by the high-energy laser pulses. In our studies, we employed PLD (PVD Products, Inc.) using a KrF excimer laser (Lambda Physik GmbH) operating at a wavelength of 248 nm for source material ablation. The Ga_2O_3 and ZnO targets were purchased from the Kurt J. Lesker Corp., with purities of 99.99% or higher. The films were deposited at 70°C, and the energy density of the laser beam at the target surface was maintained at 1.5 J/cm^2. ZnO and Ga_2O_3 targets were repeatedly ablated in a cycle consisting of a predetermined number of pulses on each of the two targets. The Ga_2O_3 doping concentration was varied in the range from 0 to 6 wt% by varying the number of ablation pulses on the Ga_2O_3 target within each cycle. In order to ensure homogeneous mixing of Ga_2O_3 in ZnO, the number of ablation pulses on each target during each cycle was kept small. Within each ablation cycle, only one pulse of laser were assigned to the Ga_2O_3 target, while a variable number of pulses (depending on the composition required) were assign to ZnO target. If an effective thickness of the resultant film deposited in each cycle was computed, the total thickness would be less than 2 nm. This ensures that the films are homogeneous and uniformly doped. Undoped films and films with 3 and 6 wt% Ga doping were prepared. The typical deposition parameters for 3 wt% and 6 wt% gallium doping are listed in Table I.

The dependence of the optical properties of the GZO films on the doping concentration was studied using a spectroscopic ellipsometer (M-2000, J.A. Woollam Co.) in the spectral region from 0.73 to 6.52 eV. In order to retrieve numerical data from the measured optical functions, we used a semi-empirical model describing the contributions of both free and bound electrons [5,8]. The Drude oscillator model is used to describe contributions of the conduction electrons that behave as free electron gas. Within the

perturbation theory, optical response from the bound electrons is well described by the oscillator model containing a set of Lorentz- or Gaussian-type single oscillators [23]. In this work, we use the Gaussian oscillator model to describe the contributions of the bound electrons. Because of the structural disorder in solid alloys, the optical functions contain a random component of optical response well described by a Gaussian distribution [24]. The following equation set presents the Drude-plus-Gaussian oscillator model:

$$\epsilon(\omega) = \epsilon_\infty - \epsilon_{\text{Drude}} + \sum_{m=1}^{n} \epsilon_{\text{Gaussian}}(\omega_m, \sigma_m) \quad (n=2), \quad (1)$$

$$\epsilon_{\text{Gaussian}}(\omega_m, \sigma_m) = \epsilon_{m1} + i\epsilon_{m2}, \quad (2)$$

$$\epsilon_{m1} = \frac{2}{\pi} P \int_0^\infty \frac{\xi \epsilon_{m2}(\xi)}{\xi^2 - \omega^2} d\xi, \quad (3)$$

$$\epsilon_{m2} = A_m e^{-\frac{(\omega-\omega_m)^2}{\sigma_m}} + A_m e^{-\frac{(\omega+\omega_m)^2}{\sigma_m}} \left(\sigma_m = \frac{\Gamma_m}{2\sqrt{\ln(2)}} \right), \quad (4)$$

$$\epsilon_{\text{Drude}} = \frac{\omega_p^2}{\omega^2 + i\Gamma_p\omega}, \quad (5)$$

where ϵ_∞ is the macroscopic dielectric permittivity, ω_p is the plasma frequency, Γ_p is the carrier relaxation rate, A_m is proportional to the oscillator strength, ω_m is the central frequency of interband electronic transitions represented by the Gaussian oscillator, and Γ_m is the broadening of the Gaussian oscillator. The extracted parameters for GZO thin films with different concentrations of gallium (undoped, 3 wt% and 6 wt%) are summarized in Table II, and Fig. 3 shows the dielectric function measured for GZO thin films. In our previous study [10], the 6 wt% was the optimum value of the doping rate to achieve the lowest drude-damping coefficient. By increasing the doping rate in the range below the optimum value, the crossover frequency becomes lower because of the increase of carrier concentration, and the optical loss becomes lower because of the improved crystallinity.

TABLE II. Extracted Drude + Gaussian oscillator parameter.

Doping rate	Undoped	3 wt%	6 wt%
ϵ_∞	2.812	2.557	2.439
ω_p	0	1.508	1.901
Γ_p	-	0.159	0.092
A_1	1.742	1.630	1.427
A_2	1.865	2.101	1.676
Γ_1	0.596	1.036	0.764
Γ_2	3.222	2.922	3.251
ω_1	3.611	4.335	4.371
ω_2	5.905	6.603	5.825
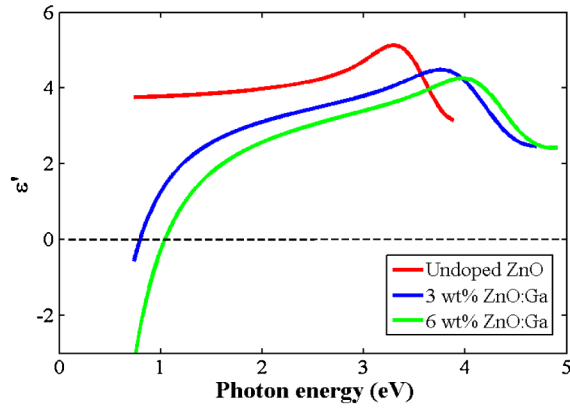
(a)
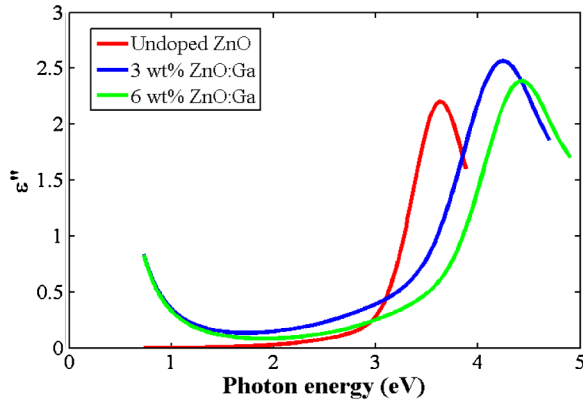
(b)

FIG. 3 (color online). Real and imaginary parts of the dielectric function spectra of w-ZnO and GZO thin films.

The structural properties of ZnO and GZO thin films were examined using x-ray diffraction (Panalytical X'Pert Pro MRD) studies with a parallel beam configuration and CuKα excitation. Figure 4 shows x-ray diffraction data ($\omega - 2\theta$ scans) of the films with different concentrations of
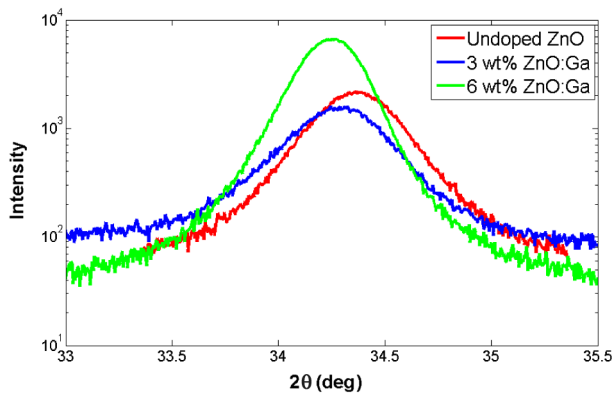

FIG. 4 (color online). X-ray diffraction ($\omega - 2\theta$) patterns for ZnO, 3 wt% GZO, and 6 wt% GZO thin films. The peak shown in the figure corresponds to 002 reflection.
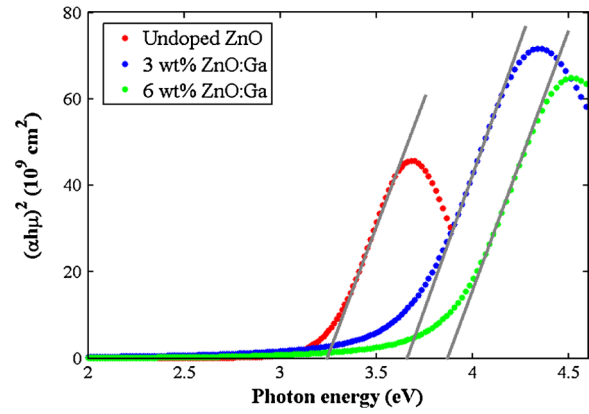

FIG. 5 (color online). Square of the absorption coefficient as a function of photon energy for ZnO, 3 wt% GZO and 6 wt% GZO thin films. E_g proportional to $(\alpha\hbar\omega)^2$ is calculated by fitting linear line to spectra E_g (Undoped ZnO):3.25 eV, E_g (3 wt% GZO):3.66 eV and E_g (6 wt% GZO):3.25 eV

gallium (undoped, 3 wt% and 6 wt%). The GZO films deposited are polycrystalline and strongly oriented along the c axis normal to the quartz substrate surface. Strong orientation of grains resulted in 002 reflection appearing around 34.5° as the only dominant peak observed [25]. In this work, only a 002 reflection peak is considered for subsequent analyses (see Fig. 4).

The optical band gap in GZO films can be determined from the spectral dependence of the absorption coefficient (α). In the direct-gap semiconductors such as ZnO, the absorption coefficient α and optical band gap (E_g) are related by Eq. (6) [26]:

$$\alpha\hbar\omega = A(\hbar\omega - E_g)^{\frac{1}{2}}, \qquad (6)$$

where $\hbar\omega$ is the incident photon energy and A is a proportionality constant. The values of E_g are extracted from the plot of α^2 vs $\hbar\omega$, as shown in Fig. 5. The E_g values are obtained from the intercept of the α^2 asymptote on the horizontal axis. This procedure results in values of E_g of 3.25 eV for undoped ZnO, and 3.66 eV and 3.89 eV for 3 wt% and 6 wt% GZO films, respectively.

III. THEORETICAL STUDIES

Heavy Ga-doped wurtzite ZnO crystals are modeled by the first-principles pseudopotential theory using the super-cell method. Equilibrium atomic structures of w-GZO are obtained from the total energy minimization method within DFT using *ab initio* pseudopotentials [27]. We employ the supercell approach to model the substitutional defects; our unit cell of GZO-$2 \times 2 \times 2$ contains 32 atoms that correspond to a new $Zn_{1-x}Ga_xO$ compound with an atomic Ga concentration of about 6 at.% ($x = 0.067$).

Ultrasoft pseudopotentials including $3d$ transition metal states in the valence band are implemented with an energy

cutoff of 420 eV. For reliable total energy convergence, $N_{\mathbf{k}}$ in the irreducible part of the brillouin zone (BZ) have been used up to $400\,\mathbf{k}$ point. With the chosen $N_{\mathbf{k}}$ and energy cutoff value, the total energy converges within a few percent. However, the density of states (DOS) convergence tests indicate that an accuracy within 5% (or better) has been achieved for DOS by using at least 1270 $\mathbf{k}$ points, as in the present work for DOS and optics.

Optical functions of GZO are calculated within the random phase approximation, as described before [23,28]. Our calculated energy gap of 0.70 eV in bulk ZnO is substantially lower than the experimental value of 3.25 eV [29]. However, it agrees well with previously reported DFT-LDA and DFT-GGA gap values [30–32]. The widely used scissor-operator correction is implemented in this calculation in order to account for the energy-gap underestimate and enable better comparison with experimental data [28,31,32]. With this method, the calculated optical spectra shift to blue.

IV. RESULTS AND DISCUSSION

Equilibrium LDA hexagonal lattice constants of bulk w-ZnO and doped GZO crystals are given in Table III.

Substitution of Ga on the Zn site (Ga_{Zn}) creates a singly occupied singlet defect state in the conduction band and thus acts as a donor in ZnO. The relaxed structure shows that in the 1^{+} state, Ga-O distances are approximately 5% to 7% shorter than corresponding values in bulk ZnO. These values agree with those reported before for the local contraction in GZO [32]. However, the fully relaxed unit cell shows some increase of the lattice constants in GZO compared with ZnO (see Table III). We considered a very high concentration of Ga in ZnO that is at the alloying level (the Ga atomic concentration is about 6% in our model). Consequently, the observed increase of the lattice constant should be related to the alloying effect.

Another important observation results from the comparison between measured and calculated x-ray diffraction (XRD) spectra. The predicted XRD spectra show a shift of $\Delta 2\theta = -0.15$ deg corresponding to the (002) reflex. This shift is comparable to the experimentally measured value of ($\Delta 2\theta = -0.1$ deg) obtained on nanocrystalline

TABLE III. Calculated and measured (in parentheses) lattice parameters of bulk ZnO and GZO.

	ZnO	GZO
a (Å)	3.213 (3.25[a])	3.296
c (Å)	5.185 (5.205[a])	5.294
a/c	1.614 (1.602[a])	1.607
2θ (deg)	36.65 (34.38[b])	36.50 (34.26[b])
$\Delta 2\theta$ (deg)	N/A	−0.15 (−0.12[b])

[a]Ref. [32].
[b]This work.

heavy doped (up to 6 at.%) GZO samples fabricated in this work (see Table III). We can state a good agreement between measured and calculated data. Note that our theoretical model does not account for any contributions of the structural disorder presented in nanocrystalline samples that may cause an observed disagreement between calculated and measured data. Therefore, within our approach the reported effect could be understood as a consequence of the unit-cell changes that may result in structural phase transformation with a further increase of Ga concentration.

A. Density of states

The calculated total densities of states (TDOS) of both bulk and Ga-doped ZnO crystals are shown in Fig. 6. Both curves are normalized with respect to the Fermi energy.

The DOS spectra of the bulk ZnO show the fully occupied Zn 3d semicore levels that are centered at about 7 eV below the valence-band maximum, in good agreement with photoemission measurement showing that the energy of maximum is −7.4 eV [33]. The upper valence band of ZnO has a predominant p-like character dominated by the O 2p orbitals, and the bottom of the conduction band is s-like and is determined by the Zn 4s orbitals.

Doping with Ga substantially modifies the density of states, generating additional occupied defect bands at and above the top of the v band (see Fig. 6). At such a very high doping concentration, these states form a new valence-band maximum that will be suitable for increasing the hole concentration. Location of this maximum is Ga-concentration dependent, which can be seen in Fig. 6. However, no remarkable difference in TDOS has been noticed between 3 and 6 wt% doped GZO, in agreement with the optical spectra measured at different concentrations (see Fig. 3). The energy shift and redistribution of the TDOS with increasing Ga concentration cause the observed variations in dielectric function spectra (see Fig. 3). Based on the
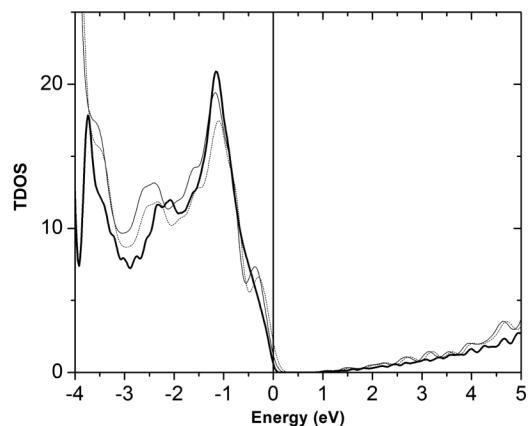

FIG. 6. Total density of states of bulk (bold line) and GZO crystal of nearly 6% (thin solid line) and 3% Ga concentration (thin dashed line).

results of this work, these changes in optical spectra are due to the rehybridization of electronic states followed by the geometry changes with increased Ga content.

Calculated band-gap values (without corrections) are $E_g = 0.70$ eV and $E_g = 0.54$ eV in undoped and Ga-doped crystals. Analysis of the total and angular-resolved DOS (see Fig. 6) indicates that the lowering of the band gap (by $\Delta E_g = -0.16$ eV) is caused by the modifications (rehybridization and renormalization) of electronic orbitals in both valence and conduction bands, as well as structural reconstruction. Comparison between DOS data obtained with unrelaxed and relaxed unit cells indicates a substantial structural reconstruction effect, which we discuss before considering the XRD data (see Table III and discussion above).

B. Optical functions

It should be noted that the DFT theory version used in this work produces the Kohn-Sham eigenenergy states that do not have a direct interpretation as the one-particle electron energy states [27]. The calculated Kohn-Sham gaps are substantially lower than measured (the "gap problem"). Consequently, the quasiparticle (QP) corrections should be introduced into the theory in order to improve comparison with experiment.

In order to compare calculated optical spectra to the measured data, the QP correction in the electronic structure model that compensates the substantial gap underestimate must be incorporated [27,31,32]. In this work, we have obtained the value of the scissor-operator correction (Δ_{sci}) from a comparison with experiment.

The calculated dielectric functions are given in Fig. 7 (for perpendicular o and parallel e polarizations). Our results are compared with experimental data obtained in bulk ZnO using the generalized ellipsometry by Jellison and
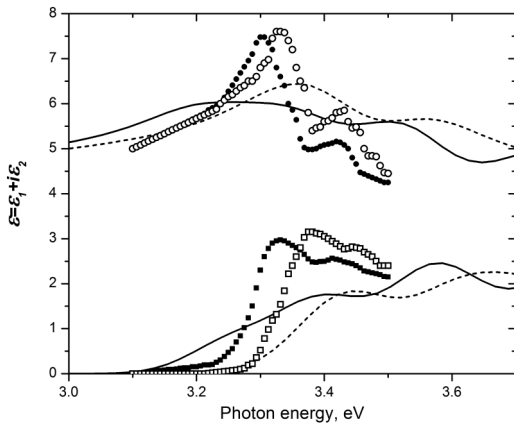

FIG. 7. Real (top of figure) and imaginary (bottom of figure) parts of the dielectric function spectra of w-ZnO bulk crystal calculated (lines) and measured (symbols) for ordinary (solid line, filled symbols) and extraordinary light (dashed line, opened symbols). Experimental data were obtained by generalized ellipsometry in Ref. [34].

Boatner [34]. From the comparison, we determined the $\Delta_{sci} = 2.55$ eV value that is used to correct the calculated spectra prior to comparing with experimental results.

Our value of $\Delta_{sci} = 2.55$ eV is comparable to the 2.70 eV used by Gori *et al.* [31]. From the comparison between calculated and measured data on bulk ZnO, we can state that our theory (DFT + Sci) correctly reproduces the measured optical anisotropy in wurtzite ZnO (see the shift between ordinary and extraordinary optical constant spectra in Fig. 7). On the other hand, this version of the theory fails to reproduce a strong peak at the absorption edge. This peak is interpreted in the literature as a consequence of a strong exciton interaction [31,35]. Inclusion of exciton effects in the band-structure calculations requires a numerical solution of the Bethe-Salpeter equation [27,28], which is very computationally expensive and out of the scope of the present work. However, as shown in this work, neglecting the exciton interaction in ZnO does not preclude us from drawing conclusions about the mechanisms that govern the optical response in doped ZnO.

Further, we consider the mechanisms that change the band gap of ZnO upon heavy doping. The measured effect of Ga doping on the optical absorption edge of GZO films is shown in Fig. 3. The contributions of plasma excitation to the dielectric function of GZO films with 3 and 6 wt% doping in the visible and near-infrared spectral regions may be observed. The variations observed are accompanied by substantial blueshifts in the optical absorption edge (see Fig. 3). The following are the main mechanisms that contribute to the optical response of such polycrystalline heavily doped semiconductor films [23]:

  i. Burstein-Moss (BM) shift
 ii. Atomic structure distortions and reconstructions
iii. Alloying effect, the electron orbital rehybridization, and transformation towards a new solid phase
 iv. Exciton effects

In this paper, we focus mostly on the changes in electron energy structure caused by heavy Ga doping. The exciton contributions are neglected because they result in an underestimation of the absolute values of $\epsilon = \epsilon_1 + i\epsilon_2$ and the absence of the characteristic peak at the fundamental absorption edge.

The BM shift describes the blueshift of the optical gap with free-carrier concentration (n) according to [29,36]

$$\Delta E_g = \frac{h^2}{8m^*}\left(\frac{3}{\pi}n\right)^{\frac{2}{3}}. \tag{7}$$

In order to understand the contribution of the doping-induced free carriers on the optical spectra in the fundamental absorption region, we calculated ΔE_g according to Eq. (7) and used it as an additional shift, together with Δ_{sci} determined for bulk ZnO (see above). Using data given in Table II for our samples, we obtained $\Delta E_g = 0.38$ and 0.52 eV for 3% and 6% Ga-doped samples, respectively.

The last value gives the scissors operator equal to $\Delta_{sci} = 3.07$ eV for 6% doped GZO.

The values of Δ_{sci} obtained for doped GZO samples are used to compare the calculated $\epsilon(\omega)$ spectra with experiment. In Fig. 8, the calculated dielectric functions are shown in comparison with experimental data for real and imaginary parts of $\epsilon(\omega)$.

We state a good overall agreement between the measured data and the results of the first-principles theory. The plasma contribution has been introduced in the theoretical model by adding the Drude term according to Eq. (5), with parameters determined experimentally (see Table II). Theoretical spectra correctly represent the shapes of the ϵ_1 and ϵ_2 curves.

Several important issues can be extracted from a comparison between calculated and measured data. There is a substantial lowering of the measured real-part values of the

(a)

(b)

FIG. 8. Real (a) and imaginary (b) parts of the dielectric function spectra of GZO samples calculated (lines) and measured (symbols) for 6 wt%.

dielectric function as a result of Ga doping (see Fig. 8). Our calculated absolute values of Re[ϵ] are lower than experimental data. The underestimation of dielectric permittivity values by first-principles theory is caused by using the exchange and correlation method and by neglecting the exciton effects described in the literature [27,28,37]. The reduction of ϵ_1 with doping is a result of the electron-energy-structure modification that includes rehybridization of electronic orbitals forming the top of the valence band and the bottom of the conduction band (see above).

Comparison between theory and experiment indicates a strong blueshift in dielectric-function spectra with an increase of Ga concentration that is substantially higher than the BM shift expected for the given Ga concentrations. The most significant difference between theory and experiment occurs at the highest-studied Ga concentration (see Fig. 8). The bulk values of $\Delta_{sci} = 2.55$ eV used to calculate theoretical $\epsilon(\omega)$ spectra are corrected on the BM shift only (0.52 eV for 6% doping). Using a calculated value of $E_g = 0.54$ eV (see above), this results in a predicted energy gap of 3.61 eV, which is substantially lower than the value of 3.89 eV measured here (see Fig. 5). Thus, the measured $\epsilon(\omega)$ spectra are remarkably blueshifted compared to the theory, as shown in Fig. 8. This clearly indicates that the BM effect is not the only mechanism responsible for the blueshift of $\epsilon(\omega)$ spectra with Ga doping.

Changes in the band structure and optical functions with the increase of the component concentration is a well-known effect in solid alloys [38]. An increase of the Ga concentration should convert GZO into Ga_2O_3 : Zn-doped oxide, i.e., through the phase transition. The crystalline $\beta - Ga_2O_3$ oxide has a monoclinic crystal structure and an optical gap in the ultraviolet region, near 4.7 eV [39,40]. It is therefore expected that the quasiparticle correction term Δ_{sci} is concentration dependent, and it will increase with the Ga concentration. Our theory does not account for any structural transformations corresponding to the phase transition. We use the super-unit-cell approach with the super-cell symmetry corresponding to that of the host ZnO. In such a way, the orbital rehybridization (alloying) effects are partially included in our model, and our results demonstrate that alloying effects are obviously important, even at only a few percent of the Ga concentration. A more advanced model should be assembled, considering possible stable (or metastable) structural phases. This highlights further developments of the GZO optics theory.

In addition, we note that both our experimental and theoretical results of the atomic structure study indicate a substantial increase of the interplanar distance in the doped samples that supports the structural mechanism contributing to the change in the optical functions with doping. The substantial underestimation of the calculated blueshift of the absorption band edge in 6 wt% GZO films against the measured value is another factor that indicates the
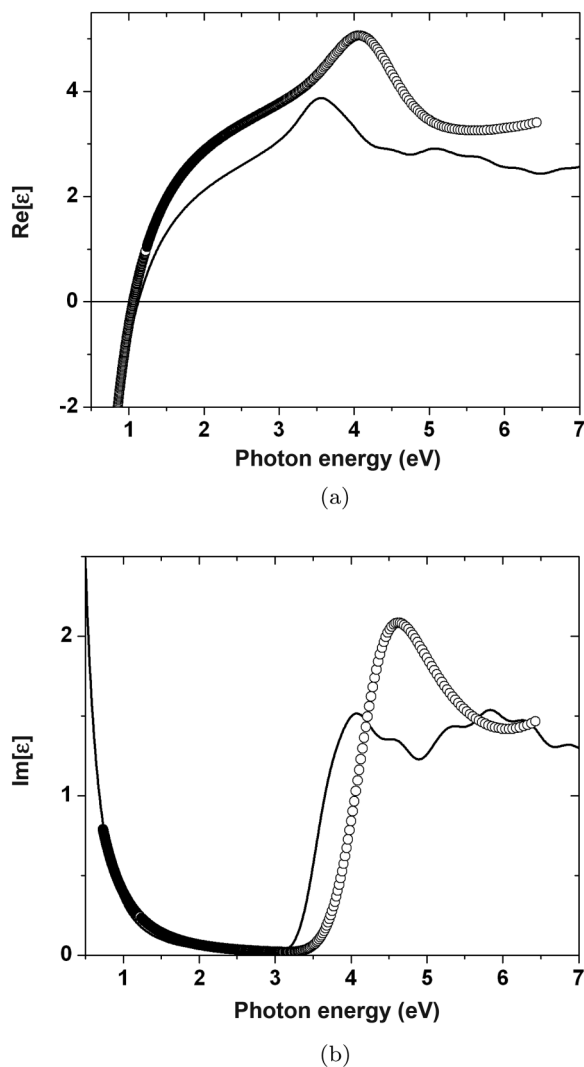
importance of the structural transformation effect, which should be accounted for by a modified theory.

V. CONCLUSIONS

We present the results of experimental and theoretical studies on the optical dielectric functions of gallium-doped ZnO polycrystalline films that are used as a low-loss plasmonic material. The comparison of dielectric functions of heavily doped GZO films extracted from ellipsometry measurements against those calculated using first-principles DFT showed that alloying effects have a significant influence on the optical properties of the films. It was shown that alloying effects are significant, even at relatively low Ga concentrations of 1 wt%. Thus, GZO that is used as a low-loss plasmonic material is not just Ga-doped ZnO but a new alloy material altogether. It was observed that a more sophisticated model is necessary to capture these alloying effects in plasmonic GZO films. This study has provided an insight into understanding the doping mechanism of heavily doped ZnO, which may be applied to other TCOs as well. Understanding the relationship between material, structural, and optical properties, as well as the physical mechanism of doping and its influence on the electronic band structure of these materials, is important for designing low-loss alternative plasmonic materials. This research direction has the potential of eventually solving the inverse-design problem of designing ultimate low-loss plasmonic building blocks that can pave the way for plasmonics and metamaterials being the next-generation technologies.

[1] D. Smith, J. Pendry, and M. Wiltshire, *Metamaterials and Negative Refractive Index*, Science **305**, 788 (2004).

[2] J. Pendry, D. Schurig, and D. Smith, *Controlling Electromagnetic Fields*, Science **312**, 1780 (2006).

[3] H. Atwater, *The Promise of Plasmonics*, Sci. Am. **296**, 56 (2007).

[4] W. Cai and V. Shalaev, *Optical Metamaterials: Fundamentals and Applications* (Springer Verlag, New York, 2009).

[5] A. Boltasseva and H. Atwater, *Low-Loss Plasmonic Metamaterials*, Science **331**, 290 (2011).

[6] J. Khurgin and G. Sun, *In Search of the Elusive Lossless Metal*, Appl. Phys. Lett. **96**, 181102 (2010).

[7] G. V. Naik, V. M. Shalaev, and A. Boltasseva, *Alternative Plasmonic Materials: Beyond Gold and Silver*, Adv. Mater. **25**, 3264 (2013).

[8] G. Naik and A. Boltasseva, *Semiconductors for Plasmonics and Metamaterials*, Phys. Status Solidi-R **4**, 295 (2010).

[9] C. Rhodes, S. Franzen, J. Maria, M. Losego, D. Leonard, B. Laughlin, G. Duscher, and S. Weibel, *Surface Plasmon Resonance in Conducting Metal Oxides*, J. Appl. Phys. **100**, 054905 (2006).

[10] G. Naik, J. Kim, and A. Boltasseva, *Oxides and Nitrides as Alternative Plasmonic Materials in the Optical Range*, Opt. Mater. Express **1**, 1090 (2011).

[11] M. Noginov, L. Gu, J. Livenere, G. Zhu, A. Pradhan, R. Mundle, M. Bahoura, Y. Barnakov, and V. Podolskiy, *Transparent Conductive Oxides: Plasmonic Materials for Telecom Wavelengths*, Appl. Phys. Lett. **99**, 021101 (2011).

[12] T. R. Gordon, T. Paik, D. R. Klein, G. V. Naik, H. Caglayan, A. Boltasseva, and C. B. Murray, *Shape Dependent Plasmonic Response and Directed Self Assembly in a New Semiconductor Building Block, Indium Doped Cadmium Oxide (ICO)*, Nano Lett. **13**, 2857 (2013).

[13] J. Kim, G. Naik, N. Emani, U. Guler, and A. Boltasseva, *Plasmonic Resonances in Nanostructured Transparent Conducting Oxide Films*, IEEE J. Sel. Top. Quantum Electron. **19**, 4601907 (2013).

[14] P. B. Johnson and R. Christy, *Optical Constants of the Noble Metals*, Phys. Rev. B **6**, 4370 (1972).

[15] P. West, S. Ishii, G. Naik, N. Emani, V. Shalaev, and A. Boltasseva, *Searching for Better Plasmonic Materials*, Laser Photonics Rev. **4**, 795 (2010).

[16] M. G. Blaber, M. D. Arnold, and M. J. Ford, *Designing Materials for Plasmonic Systems: The Alkali-Noble Intermetallics*, J. Phys. Condens. Matter **22**, 095501 (2010).

[17] D. A. Bobb, G. Zhu, M. Mayy, A. V. Gavrilenko, P. Mead, V. I. Gavrilenko, and M. A. Noginov, *Engineering of Low-Loss Metal for Nanoplasmonic and Metamaterials Applications* , Appl. Phys. Lett. **95**, 151102 (2009).

[18] M. Yoon, S. Lee, H. Park, H. Kim, and M. Jang, *Solid Solubility Limits of Ga and Al in ZnO*, J. Mater. Sci. Lett. **21**, 1703 (2002).

[19] H. Kim, C. Gilmore, A. Pique, J. Horwitz, H. Mattoussi, H. Murata, Z. Kafafi, and D. Chrisey, *Electrical, Optical, and Structural Properties of Indium-Tin-Oxide Thin Films for Organic Light-Emitting Devices*, J. Appl. Phys. **86**, 6451 (1999).

[20] K. Postava, H. Sueki, M. Aoyama, T. Yamaguchi, K. Murakami, and Y. Igasaki, *Doping Effects on Optical Properties of Epitaxial ZnO Layers Determined by Spectroscopic Ellipsometry*, Appl. Surf. Sci. **175**, 543 (2001).

[21] F. Shan and Y. Yu, *Optical Properties of Pure and Al Doped ZnO Thin Films Fabricated with Plasma Produced by Excimer Laser*, Thin Solid Films **435**, 174 (2003).

[22] S. M. Park, T. Ikegami, and K. Ebihara, *Effects of Substrate Temperature on the Properties of Ga-Doped ZnO by Pulsed Laser Deposition*, Thin Solid Films **513**, 90 (2006).

[23] V. I. Gavrilenko, *Optics of Nanomaterials* (Pan Stanford Publishing, Singapore, 2011).

[24] P. D. Paulson, R. W. Birkmire, and W. N. Shafarman, *Optical Characterization of* $CuIn_{1-x}Ga_xSe_2$ *Alloy Thin*

Films by Spectroscopic Ellipsometry, J. Appl. Phys. **94**, 879 (2003).

[25] Y. Kajikawa, *Texture Development of Non-epitaxial Polycrystalline ZnO Films*, J. Cryst. Growth **289**, 387 (2006).

[26] G. Dresselhaus, *Optical Absorption Band Edge in Anisotropic Crystals*, Phys. Rev. **105**, 135 (1957).

[27] R. M. Martin, *Electronic Structure. Basic Theory and Practical Methods* (Cambridge University Press, Cambridge, England, 2004).

[28] V. I. Gavrilenko and F. Bechstedt, *Optical Functions of Semiconductors Beyond Density Functional Theory*, Phys. Rev. B **55**, 4343 (1997).

[29] J H. Noh, H. S. Jung, J.-K. Lee, J. Y. Kim, C. M. Cho, J.-S. An, and K. S. Hong, *Reversible Change in Electrical and Optical Properties in Epitaxially Grown Al-Doped ZnO Thin Films*, Appl. Phys. Lett. **104**, 073706 (2008).

[30] M. Usuda, N. Hamada, T. Kotani, and M. van Schilfgaarde, *All Electron GW Calculation Based on the LAPW Method: Application to wurtzite ZnO*, Phys. Rev. B **66**, 125101 (2002).

[31] P. Gori, M. Rakel, C. Cobert, W. Richter, N. Esser, A. Hoffmann, R. D. Sole, A. Cricenti, and O. Pulci, *Optical Spectra of ZnO in the Far Ultraviolet: First- Principles Calculations and Ellipsometric Measurements*, Phys. Rev. B **81**, 125201 (2010).

[32] X. M. Duan, C. Stampfl, M. M. M. Bilek, and D. R. McKenzie, *Codoping of Aluminum and Galium with Nitrogen in ZnO: A Comparative First-Principles Iinvestigation*, Phys. Rev. B **79**, 235208 (2009).

[33] A. R. H. Preston, B. J. Ruck, L. F. J. Piper, A. DeMasi, K. E. Smith, A. Schleife, F. Fuchs, F. Bechstedt, J. Chai, and S. M. Durbin, *Band Structure of ZnO from Resonant X-Ray Emission Spectroscopy*, Phys. Rev. B **78**, 155114 (2008).

[34] J. G. E. Jellison and L. A. Boatner, *Optical Functions of Uniaxial ZnO Determined by Generalized Ellipsometry*, Phys. Rev. B **58**, 3586 (1998).

[35] J. F. Muth, R. M. Kolbas, A. K. Sharma, S. Oktyabrsky, and J. Narayan, *Excitonic Structure and Absorption Coeffecient Measurements of ZnO Single Crystal Epitaxial Films Deposited by Pulsed Laser Deposition*, J. Appl. Phys. **85**, 7884 (1999).

[36] E. Burstein, *Anoma1ous Optical Absorption Limit in InSb*, Phys. Rev. **93**, 632 (1954).

[37] V. I. Gavrilenko, in *Tutorials in Complex Photonic Media*, edited by M. A. Noginov, M. W. McCall, G. Dewar, and N. I. Zheludev (SPIE Press, Bellingham, 2009), Chap. 15, pp. 479–524.

[38] I. Vurgaftman, J. R. Meyer, and L. R. Ram-Mohan, *Band Parameters for III-V Compound Semiconductors and Their Alloys*, J. Appl. Phys. **89**, 5815 (2001).

[39] M. Yamaga, E. G. Víllora, K. Shimamura, N. Ichinose, and M. Honda, *Donor Structure and Electric Transport Mechanism in $\beta - Ga_2O_3$*, Phys. Rev. B **68**, 155207 (2003).

[40] Y. Zhang, J. Yan, G. Zhao, and W. Xie, *First-Principles Study on Electronic Structure and Optical Properties of Sn-doped $\beta - Ga_2O_3$*, Physica (Amsterdam) **405B**, 3899 (2010).